minerals

MDPI

Article

Geochemistry, Zircon U–Pb Age, and Lu–Hf Isotope of the Granite Porphyry in Leimengou Mo Deposit in the East Qinling Molybdenum Ore Belt, China

Jing Cao [1], Huishou Ye [2,*], Xiaodan Chen [2], Wen He [1] and Peng Wang [1]

[1] School of Earth Sciences and Resources, China University of Geosciences, Beijing 100083, China; 13716896907@163.com (J.C.); wenhe1843@126.com (W.H.); PengWangvip@163.com (P.W.)

[2] MLR Key Laboratory of Metallogeny and Mineral Assessment, Institute of Mineral Resources, Chinese Academy of Geological Sciences, Beijing 100037, China; chenxdxd@126.com

* Correspondence: 3001140024@cugb.edu.cn

Received: 25 April 2018; Accepted: 27 June 2018; Published: 10 July 2018

Abstract: The Leimengou Mo deposit is one of the typical porphyry deposits in the East Qinling molybdenum ore belt. The Mo mineralization mainly hosts in the Leimengou intrusion, with minor by the gneiss of Archean Taihua Group. The Leimengou intrusion is composed of granite porphyry and monzonitic granite porphyry. Zircon U–Pb LA-(MC)-ICP-MS dating of the two rocks yield the same age of 131 ± 0.6 Ma (N = 23, MSWD = 1.6), consistent with 132 ± 2 Ma of Mo mineralization age obtained by the Re–Os method. The Leimengou intrusion is peraluminous (A/CNK = 1.06–1.28) and high-K calc-alkaline series ($K_2O + Na_2O$ = 7.84%–9.07%). The REE and trace elements are enriched in large ion lithophile elements (LREE, K, Rb, Ba, Sr, Th and U), and depleted in high-field strength elements (HREE, Nb, Ti and P), with moderately negative abnormal of Eu. Both granite porphyry and monzonitic granite porphyry show a large variation in zircon Hf isotopic compositions with $\varepsilon_{Hf}(t)$ values of −27.9 to −16.9 and −26.0 to −15.2, and two-stage model ages of 2259 to 2946 Ma and 2149 to 2827 Ma, respectively. Whole rock geochemistry and zircon Lu–Hf isotopic compositions suggest that the Leimengou intrusion was derived mainly from an ancient continental crust (probably Archean Taihua Group), with the addition of mantle-derived components.

Keywords: zircon U–Pb dating; Lu–Hf isotope; granite porphyry; Leimengou; Southern margin of North China Block

1. Introduction

The East Qinling molybdenum ore belt, located on the southern margin of the North China Block, is one of the most important molybdenum polymetallic metallogenic belts in China. There are seven super large Mo deposits such as Jinduicheng, Nannihu-Sandaozhuang and Donggou, and more than 10 large and medium-sized Mo deposits such as Leimengou deposit in the ore belt. The most Mo deposits belong to porphyry (-skarn) type, which are closely related to the Yanshanian small-scale intermediate-acidic porphyry intrusions [1]. The ore belt also accommodates many Yanshanian batholiths, including Laoniushan, Huashan, Wenyu, Niangniangshan, Huashan, Wuzhangshan, etc. (Figure 1), which are contemporary with the porphyry (-skarn) Mo deposits and ore-related porphyry intrusions. Spatially, these Mo-bearing porphyry intrusions are generally distributed around the ore-free batholiths. For example, Jinduicheng, Shijiawan, Balipo porphyries and their related Mo deposits emplaced around the Laoniushan batholith, the Leimengou and Shapoling porphyry Mo deposits are located on the east and west sides of the Huashan batholith, respectively, the Donggou super large Mo deposit and related Donggou granite porphyry are located on the north side of the Taishanmiao batholith. Besides, the Donggou granite porphyry is considered as the branch of Taishanmiao batholith or the late

product of its differentiation [2,3]. In terms of time, these Mo-bearing porphyry intrusions have consistent ages with their adjacent batholiths. Geochemical studies in recent years have shown that these ore-related porphyries are genetically correlated to their adjacent batholiths, and that they have the same source region [4,5], and may have magma evolution relationship [2,3,6].

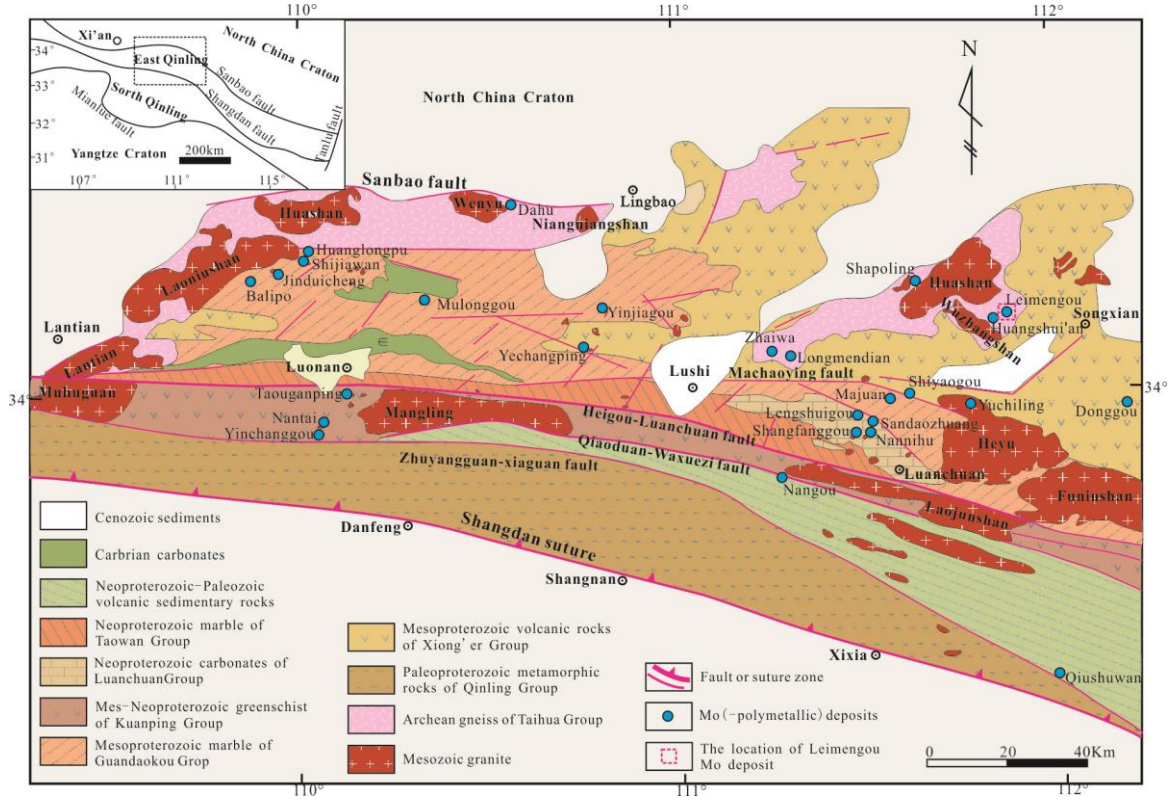

Figure 1. Distribution pattern of the late Mesozoic intrusions in the East Qinling orogenic belt (modified after Mao et al., 2010 [7]).

The Leimengou Mo deposit is one of the typical porphyry Mo deposits in the East Qinling area. The deposit is located in the Xiongershan area in the eastern section of the East Qinling molybdenum ore belt and is about six km away from the eastern side of the Huashan granite batholith. The molybdenum resources is more than 34×10^4 t, and the average Mo grade is 0.07% [8] ,belonging to a large scale deposit. Previous studies involved investigations of detailed deposit geology, chronology [9], and ore-forming fluids [8]. However, some issues still remained to be solved. On the one hand, Li et al. (2006) [9] obtained the SHRIMP zircon U–Pb age of 136.2 ± 1.5 Ma for the Leimengou granite porphyry, and molybdenite Re–Os age of 132.4 ± 1.9 Ma for Leimengou Mo deposit. It seems that the Leimengou granite porphyry was generated earlier than Leimengou Mo deposit by 4 Ma, therefore further geochronological work is necessary to define it. In addition, for the zircon U–Pb age of the Leimengou granite porphyry is older than that of the adjacent Huashan granite (the SHRIMP zircon U–Pb age is 131 ± 1–132 ± 2 Ma [7], the Leimengou Mo deposit and ore-related granite porphyry was considered not to be associated with the Huashan batholith [9,10]. This is inconsistent with the ubiquitous spatial-temporal correlation between the Mo-bearing porphyries and their adjacent granite batholiths in the East Qinling molybdenum belt mentioned above. Therefore, it is necessary to further verify the age of the Leimengou granite porphyry. On the other hand, in spite of a small scale, the Leimengou granite intrusion is closely related to Mo mineralization. The lack of geochemical and isotope research has limited the understanding of its material source and magma source region. Therefore, on the basis of previous studies, the authors carried out the research on the Leimengou granite intrusion in terms of the geochemistry, LA-(MC)-ICP-MS zircon

U–Pb dating, and Lu–Hf isotope to further define the age of the intrusion, determine the geochemical compositions, and discuss the material sources.

2. Regional Geology

The southern margin of the North China Block, where the Leimengou Mo deposit is located, is the hinterland thrust-and-fold belt of the Qinling orogenic belt [11]. In the north, it is adjacent to the North China Block, bordered by the Sanbao fault. In the south, it is in contact with the Proterozoic Kuanping Group of the North Qinling Middle-Upper, and bounded by the Heigou–Luanchuan fault (Figure 1). The strata within the area include Archean high-grade metamorphic rocks of the Taihua Group, Mesoproterozoic metavolcanic rocks of the Xiong'er group, Mesoproterozoic to Neoproterozoic marine sedimentary rocks, Cambrian carbonate and Cenozoic cover.

The regional faults are developed, mainly in the east-west and north-east directions (Figure 1). The boundary faults are represented by the east–west Machaoying fault and the Heigou–Luanchuan fault. The north-east fault is superimposed on the east-west fault. The intersection of the two faults controls the distribution of the intermediate porphyries in the Yanshanian period. The igneous rocks are widely developed and the Yanshanian granitic magmatism activity is the most intense. Yanshanian granites emplaced in two forms, one is a large batholith, such as Laoniushan, Huashan, Wenyu, Niangniangshan, Huashan, Wuzhangshan, Funiushan, for example; the other is a small porphyry intrusion, such as Jinduicheng, Shijiawan, Babaoshan, Nannihu, Huoshenmiao, Leimengou, for example. These small porphyry intrusions are closely related to Mo mineralization and therefore constitute the famous East Qinling molybdenum belt. These Late Mesozoic granitic magmatism can be divided into two stages: late Jurassic-Early Cretaceous (160–130 Ma) and middle and late Cretaceous (120–100 Ma) [12]. On the southern margin of the North China Block, diagenesis and metallogenesis are spatially and temporally consistent.

The Leimengou Mo deposit is located on the east side of Huashan and Wuzhangshan batholith (Figure 1). The Huashan batholith is about 6 km away from the northwest side of the mining area. The exposed area is more than 300 km^2. It has irregularly intruded into the Taihua Group and locally invaded the Xiong'er group. Huashan batholith is a multi-stage intrusive complex consisting of Huashan, Haopingping and Jinshanmiao rock intrusions. The lithologies are mainly porphyritic-like biotite-hornblende monzonitic granite, medium-fine grained biotite monzogranite, and porphyritic-like plagioclase-bearing quartz porphyry [13], and the former two types of lithology constitute the main body of the batholith. Mao et al. (2010) [7] obtained SHRIMP zircon U–Pb ages of 132.0 ± 1.6 Ma and 130.7 ± 1.4 Ma for the Huashan and Haopingping granite of the Huashan batholith, respectively; Xiao et al. (2012) [14] obtained LA-ICP-MS zircon U–Pb ages of 128.7 ± 1.0 Ma to 129.3 ± 2.4 Ma for the Haoping and Jinshanmiao granite of the Huashan batholith, respectively. Around the Huashan granite batholith, numerous granite intrusions, dykes and cryptoexplosive breccia emplaced, besides Leimengou Mo deposit, the gold deposits, Qiyugou, Shanggong, Hugou, etc., also develop around the Huashan granite batholith, of which the Qiyugou gold deposit is considered to be related to the Yanshanian magma and hydrotherm activity [15].

The Wuzhangshan granite batholith is distributed in the southwestern part of the mining area, with an exposed area of about 58 km^2. It has a northwest-southeastward plate-like extension in the region. The main lithology is a porphyritic-like biotite-hornblende monzonitic granite. It has SHRIMP zircon U–Pb age of 157 ± 1 Ma [7]. The granite dykes are developed around the Wuzhangshan batholith.

3. Deposit Geology and Petrography

3.1. Deposit Geology

The exposed strata in the mining area are mainly gneiss of the Archean Taihua Group (Figure 2). The main lithologies are biotite plagioclase gneiss, hornblende plagioclase gneiss, and biotite-hornblende

plagioclase gneiss. The middle-late Proterozoic and Yanshanian igneous rocks are developed in the mining area. The Proterozoic igneous rocks are dominated by mafic dykes, which mainly consist of gabbro diabase and dacite-porphyrite. The Yanshanian igneous group is mainly intermediate-acid intrusions, including syenite porphyry dykes, quartz porphyry dykes, monzonitic granite porphyry dykes, granite porphyry intrusion and crypto-explosive breccia (Figure 2). The LA-ICP-MS zircon U–Pb ages of the monzonitic granite porphyry dykes, quartz porphyry dikes are 124 ± 0.6 Ma (forthcoming data) and 127 ± 1 Ma [8], respectively, and the SHRIMP zircon U–Pb age of the granite porphyry is 136 ± 2 Ma [9].The syenite porphyry dykes are cut by granite porphyry intrusion and quartz porphyries. The granite porphyry has invaded the surrounding strata, forming crypto-explosive breccia due to cryptoexplosion. The granite porphyry intrusion and crypto-explosive breccia are closely correlated to the Mo mineralization in terms of space and time.

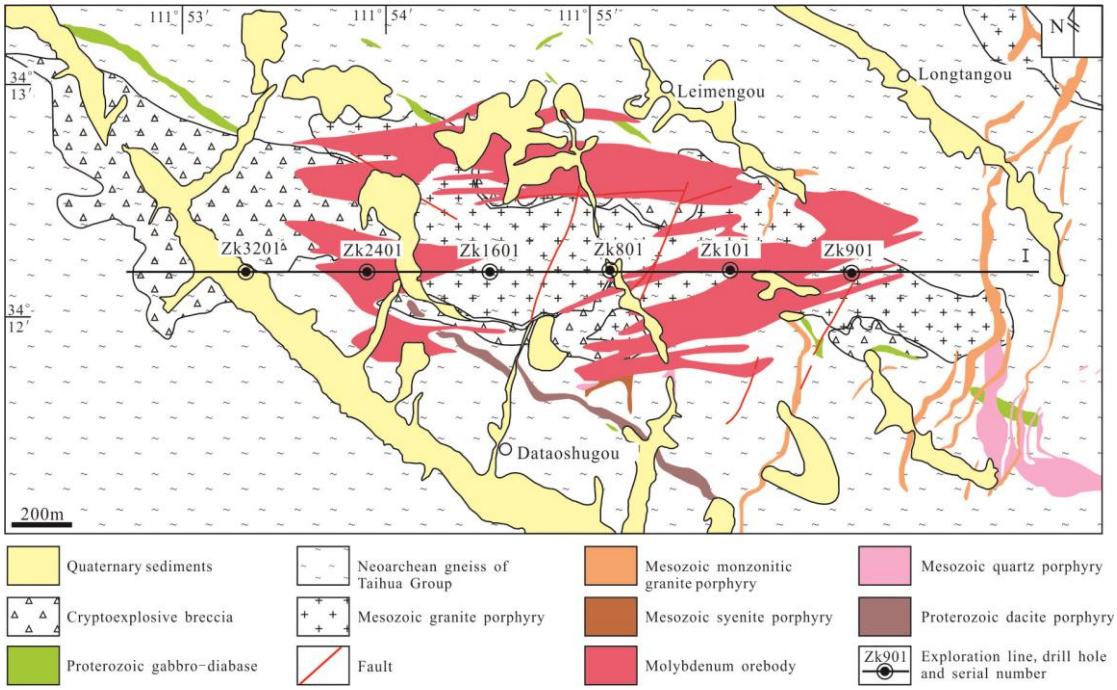

Figure 2. Geological sketch map of Leimengou Mo deposit (after Chen et al., 2011 [8]).

There are no large fold structures in the mining area, but the fault structures are relatively developed, mainly including four groups, namely the near east-west, north-north-east, north-east, and north-west groups. Among them, the north-north-east faults are the most developed, characterized by being strong in the east and weak in the west, which cut through the Leimengou granite porphyry in the eastern part of the mining area and cut off the east-west faults locally. Most of the faults have obvious compression and torsion characteristics and are filled by later dykes.

The Mo ore body occurred near the inner and outer contact zone of Leimengou granite intrusion and Taihua group gneiss, and is concentrated within 0–600 m of the inner contact zone and 0–300 m of the outer contact zone (Figures 2 and 3). Mo mineralization is weakened toward inner and outer sides. The Mo ore body has a semi-circular opening in the southern part from the perspective of the plane, and shows a layered, lenticular shape in the cross-section, with the near east-west tendency, a flat dip, and a relatively steep dip angle in some parts (Figure 3). The ore minerals are mainly molybdenite and pyrite, containing a small amount of chalcopyrite, galenite, sphalerite, etc.; and the gangue minerals are mainly quartz, potassium feldspar, plagioclase, sericite, biotite. The molybdenite mainly occurs as disseminations, veinlets and stockworks.

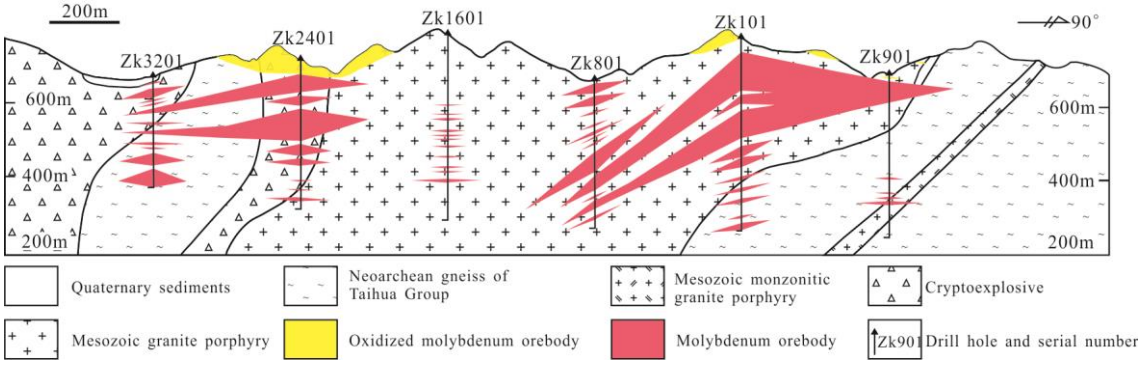

Figure 3. Geological section along No. I exploration line of Leimengou Mo deposit (after Chen et al., 2011 [8]).

The wall rock alterations include potash feldspathization, silicification, sericitization, fluoritization, chloritization, carbonatation, kaolinization. Potassium feldspar, the predominant hydrothermal mineral, is mainly distributed in the granite porphyry in the internal contact zone. The silicification is mainly developed in the contact zone near the inside of the Leimengou granite inrusion, and the sericitization alteration is often superimposed above the potassium feldspar and silicification alterations.

3.2. Petrography

The Leimengou porphyry is of small intrusion, showing an EW spindle-like shape in the plane (Figure 2). The intrusion starts from the Leimengou delta point in the east, passing through Leimengou, Jingquangou, Taoshugou till to Nianpangou, and the surface part is as long as 2210 m, and the north-south width is about 200 to 450 m, with the exposed area of about 0.77 km^2. In the section, the granite porphyry steeply inclined inwardly and occurs as a westward funnel (Figure 3).

The crypto-explosive breccia, which has a direct genetic association with the intrusion, intermittently occurred on the edge of the intrusion. The intrusion is undulating or irregular bay-like, and the contact boundary with the wall rock is clear. The contact zone has alteration and mineralization in different degrees, mainly including silicification, potash feldspathization, sericitization and pyrite and molybdenite mineralization. The granite porphyry in the shallow part of the intrusion is light red, blocky, and patchy (Figure 4a). The granite porphyry is composed of potassium feldspar (40% to 50%), quartz (35% to 40%) coma plagioclase (15% to 25%), and biotite (5%). The accessory minerals are magnetite, ilmenite, rutile and zircon. Among them, the phenocrysts account for about 10% to 15%, including potassium feldspar, quartz, plagioclase and a small amount of biotite (Figure 4b). The potassium feldspar phenocryst is of subhedral-anhedral plate shape, with a grain size of 1 to 4 mm and a maximum of 6 mm. Quartz crystals are mostly anhedral granular and have a grain size of 2 to 5 mm with wavy extinction. The particle size of plagioclase phenocrysts varies greatly, mostly ranging from 2 mm to 6 mm, and sericitization occurred on the surface in most cases (Figure 4c). The matrix is mainly quartz, potassium feldspar, and a small amount of biotite. Due to the strong potassium feldspar and silicification alterations, it presents micrograined crystalloblastic texture.

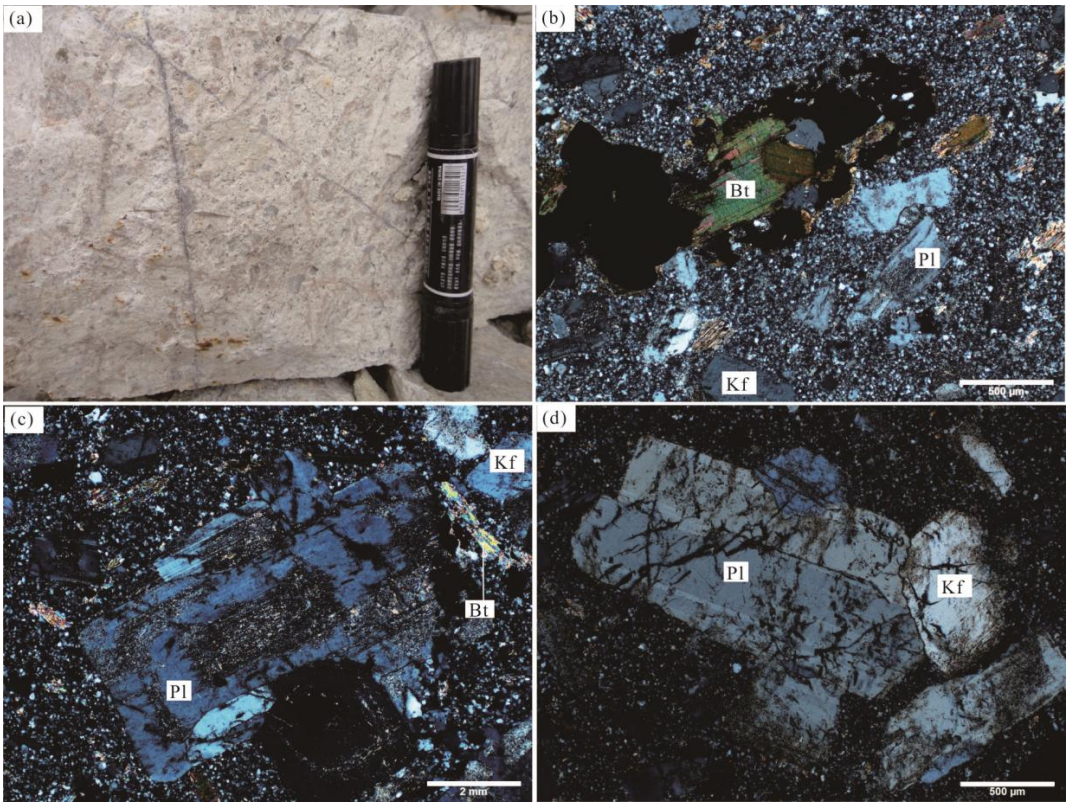

Figure 4. Hand specimens and photomicrographs showing petrology of Leimengou granite porphyry and monzonitic granite porphyry. Bt—biotite; Kf—feldspar; Pl—plagioclase.

The lithology gradually transits to monzonitic granite porphyry with the intrusion extending to deep site. The rocks are grayish white, with a massive structure and porphyritic texture. The phenocryst content increases to 25% to 35%, including potassium feldspar (10% to 25%) and plagioclase (10% to 20%) and minor quartz. The phenocryst is mostly of subhedral plate shape (Figure 4d), and the matrix is micro-fine to fine grained textures.

4. Samples and Analysis Methods

4.1. Samples

The samples used for the zircon U–Pb dating are weakly-mineralized granite porphyry (No. LMG-B15) and monzonitic granite porphyry (No. LMG-B5). Weak sericitization occurred on the surface of potassium feldspar and plagioclase phenocrysts. Five non-mineralized and non-altered granite porphyry samples (No. B16/LMG to B20/LMG) were taken from the open pit in the Leimengou mining area and from different locations of the Leimengou granite porphyry. Six non-mineralized and non-altered monzonitic granite porphyry samples (No. B7/LMG to B12/LMG) were taken from the drill holl in the Leimengou mining area for geochemical analysis. The eleven fresh samples were taken for whole rock geochemical analysis.

4.2. Whole Rock Geochemical Analysis

The analysis of major and trace elements was performed at the National Research Center for Geoanalosis, Beijing, China. The major elements were determined by X-ray fluorescence spectrometry (XRF), the accuracy was better than 1%, and trace elements were analyzed with the ICP-MS, with the accuracy above 5%, and the analysis accuracy of a tiny amount of elements ($<10^{-8}$) was better than 10%.

4.3. Zircon U–Pb Dating

The zircon sorting work was completed in the Rock and Mineral Experimental Testing Center of Geological Surveying and Mapping Institute of Hebei Province. The zircon cathodoluminescence (CL) photography was conducted at the Beijing SHRIMP Center (BJSHRIMP), CAGS, China Zircon U–Pb isotopes and Hf isotopic analysis were all carried out at the Key Laboratory of Mineral Resources and Resource Assessment, Ministry of Land and Resources, Institute of Mineral Resources, Chinese Academy of Geological Sciences. The instrument used for zircon dating is a Finnigan Neptune type MC-ICP-MS and its associated New wave UP 213 laser ablation system.

The laser ablation spot diameter was 25 μm, the frequency was 10 Hz, and the density of the power was about 2.5 J/cm^2. The He-Ar gas mixture was used as the carrier gas. An analytical approach was undertaken where 5–7 measurements of unknown zircons were conducted between three measurements of GJ-1 [16] (n = 2) and Plesovice [17] (n = 1) standard zircons. The U and Th were corrected with the zircon M127 U of 923 × 10^{-6}; Th of 439 × 10^{-6} and Th/U ratio of 0.475 [18] as the external standard. The data processing was performed using the ICPMSDataCal program [16], and the zircon age harmonic diagram was obtained using the Isoplot 3.0 program. For the detailed quartz testing process, refer to the reference by Hou et al. (2009) [19].

The zircon Lu–Hf isotope test was also performed on the Finnigan Neptune multi-collector plasma spectrometry and New Wave Research UP 213 ultraviolet laser ablation system (LA-MC-ICP-MS). Helium was used as an ablation carrier gas with an ablation diameter of 55 μm. The ablation time was 60 s. The zircon international standard GJ1 was used as a reference material for the test, and the analysis point was at the same position as the U–Pb dating point. For related instrument operating conditions and detailed analysis procedures, please refer to the reference by Hou et al. (2007) [20]. The weighted average of the $^{176}Hf/^{177}Hf$ test of the zircon standard GJ1 during the analysis was 0.282015 ± 28 (2σ, n = 10), which is in accordance with the reported values (0.282008 ± 25) [20,21] within the error range.

5. Results

5.1. Zircon U–Pb Geochronology

The zircons selected from the Leimengou granite porphyry and monzonitic granite porphyry are similar in shape and size. They are mostly colorless and transparent, and some are slightly yellowish. The crystals are mostly subhedral-anhedral columns with short to long length, and a few are purplish. The sizes of the zircons are generally 60 to 150 μm, and the length–width ratio is generally 2:1 to 3:1. The zircons have complete, straight and smooth crystal surface. The cathodoluminescence (CL) image (Figure 5) shows that the representative zircons have a typical magmatic concentric oscillatory zoning, reflecting the structural characteristics of the magmatic zircon. The U and Th contents of zircons in the granite porphyry vary from 103 × 10^{-6} to 1946 × 10^{-6} and 81 × 10^{-6} to 2186 × 10^{-6}, respectively, while the values change from 148 × 10^{-6} to 2345 × 10^{-6} and 218 × 10^{-6} to 3167 × 10^{-6}, respectively, in the monzonitic granite porphyry. The Th/U ratio of the two rocks is 0.44 to 2.16 and 0.43 to 2.45, respectively (Table 1). The above characteristics indicate that the zircon of the Leimengou granite porphyry and monzonitic granite porphyry is of magma genesis. The results from 25 measurement points in the granite porphyry sample (LMG-B15) and 23 measurement points in the monzonitic granite porphyry sample (LMG-B5) all fell on and near the Concordia line, respectively (Figure 6), and yield the same weighted average age of 131 ± 0.6 Ma (MSWD = 1.6), representing the crystallization age of the Leimengou granite porphyry and monzonitic granite porphyry.

Table 1. LA-(MC)-ICP-MS zircon U–Pb data of the Leimengou granite porphyry (LMG-B15) and monzonitic granite porphyry (LMG-B5).

Sample No.	Pb × 10^{-6}	Th × 10^{-6}	U × 10^{-6}	Th/U	Isotope Ratio						Age (Ma)					
					$^{207}Pb/^{206}Pb$	1σ	$^{207}Pb/^{235}U$	1σ	$^{206}Pb/^{238}U$	1σ	$^{207}Pb/^{206}Pb$	1σ	$^{207}Pb/^{235}U$	1σ	$^{206}Pb/^{238}U$	1σ
LMG-B15-1	375	615	1161	0.55	0.0487	0.0005	0.1363	0.0017	0.0203	0.0001	132	31	130	1	129	1
LMG-B15-2	502	807	561	1.44	0.0494	0.0008	0.1408	0.0023	0.0207	0.0002	169	40	134	2	132	1
LMG-B15-3	455	769	1158	0.67	0.0493	0.0006	0.1393	0.0020	0.0205	0.0002	161	31	132	2	131	1
LMG-B15-4	456	881	1180	0.75	0.0488	0.0006	0.1395	0.0020	0.0207	0.0001	139	30	133	2	132	1
LMG-B15-5	356	600	1083	0.55	0.0500	0.0007	0.1404	0.0021	0.0204	0.0001	195	36	133	2	130	1
LMG-B15-6	1042	1921	1925	1.00	0.0511	0.0008	0.1463	0.0023	0.0208	0.0001	256	35	139	2	133	1
LMG-B15-7	708	1213	1572	0.77	0.0488	0.0005	0.1399	0.0018	0.0208	0.0002	200	26	133	2	133	1
LMG-B15-8	540	926	1093	0.85	0.0487	0.0007	0.1380	0.0022	0.0206	0.0002	200	35	131	2	131	1
LMG-B15-9	921	1631	1760	0.93	0.0489	0.0010	0.1395	0.0033	0.0206	0.0002	143	48	133	3	132	1
LMG-B15-10	553	722	1307	0.55	0.0497	0.0006	0.1423	0.0021	0.0208	0.0002	189	31	135	2	133	1
LMG-B15-11	504	1020	1431	0.71	0.0487	0.0007	0.1359	0.0021	0.0203	0.0002	200	33	129	2	129	1
LMG-B15-12	658	976	1493	0.65	0.0492	0.0007	0.1372	0.0022	0.0202	0.0001	167	35	131	2	129	1
LMG-B15-13	315	333	230	1.45	0.0496	0.0019	0.1381	0.0062	0.0202	0.0006	176	91	131	6	129	4
LMG-B15-14	317	624	681	0.92	0.0510	0.0007	0.1436	0.0039	0.0204	0.0005	243	30	136	3	130	3
LMG-B15-15	103	241	172	1.40	0.0510	0.0015	0.1441	0.0067	0.0204	0.0006	239	69	137	6	130	4
LMG-B15-16	1242	1946	2186	0.89	0.0489	0.0009	0.1406	0.0028	0.0208	0.0001	143	43	134	2	133	1
LMG-B15-17	154	284	132	2.16	0.0515	0.0024	0.1424	0.0055	0.0203	0.0004	265	107	135	5	129	2
LMG-B15-18	453	925	1078	0.86	0.0494	0.0029	0.1381	0.0073	0.0203	0.0005	165	131	131	6	130	3
LMG-B15-19	179	277	627	0.44	0.0505	0.0007	0.1434	0.0022	0.0207	0.0002	220	33	136	2	132	1
LMG-B15-20	474	631	562	1.12	0.0488	0.0007	0.1405	0.0024	0.0209	0.0002	139	33	133	2	134	1
LMG-B15-21	193	103	81	1.28	0.0509	0.0029	0.1476	0.0088	0.0211	0.0006	235	133	140	8	134	4
LMG-B15-22	360	289	167	1.73	0.0500	0.0013	0.1386	0.0038	0.0203	0.0003	195	61	132	3	130	2
LMG-B15-23	591	403	356	1.13	0.0504	0.0008	0.1412	0.0023	0.0203	0.0002	213	31	134	2	130	1
LMG-B15-24	898	719	1456	0.49	0.0492	0.0005	0.1386	0.0018	0.0204	0.0002	167	-6	132	2	130	1
LMG-B15-25	2730	1774	2150	0.83	0.0498	0.0005	0.1423	0.0020	0.0207	0.0002	187	26	135	2	132	1
LMG-B5-1	86	492	677	0.73	0.0517	0.0015	0.1464	0.0045	0.0207	0.0002	272	67	139	4	132	2
LMG-B5-2	194	918	1346	0.68	0.0495	0.0008	0.1420	0.0025	0.0209	0.0001	169	37	135	2	134	1
LMG-B5-3	140	557	1113	0.50	0.0497	0.0007	0.1427	0.0020	0.0209	0.0001	189	30	135	2	133	1
LMG-B5-4	172	787	1542	0.51	0.0513	0.0008	0.1439	0.0023	0.0204	0.0002	254	33	137	2	130	1
LMG-B5-5	44	218	501	0.43	0.0491	0.0009	0.1380	0.0027	0.0204	0.0002	154	36	131	2	130	1
LMG-B5-6	177	883	1417	0.62	0.0489	0.0007	0.1373	0.0022	0.0204	0.0002	146	40	131	2	130	1
LMG-B5-7	27	292	471	0.62	0.0489	0.0007	0.1367	0.0023	0.0203	0.0002	139	31	130	2	130	1
LMG-B5-8	360	2033	2345	0.87	0.0492	0.0006	0.1401	0.0021	0.0207	0.0002	167	28	133	2	132	1
LMG-B5-9	218	1265	1904	0.66	0.0492	0.0009	0.1379	0.0028	0.0203	0.0001	167	44	131	3	130	1
LMG-B5-10	171	1025	1663	0.62	0.0502	0.0008	0.1402	0.0027	0.0203	0.0001	206	39	133	2	129	1
LMG-B5-11	430	3167	2067	1.53	0.0497	0.0013	0.1416	0.0051	0.0204	0.0002	189	59	134	5	130	1
LMG-B5-12	455	233	148	1.58	0.0493	0.0019	0.1390	0.0054	0.0205	0.0002	165	88	132	5	131	1
LMG-B5-13	301	1965	1992	0.99	0.0508	0.0009	0.1438	0.0029	0.0206	0.0002	232	41	136	3	131	1
LMG-B5-14	254	2009	2123	0.95	0.0493	0.0012	0.1392	0.0042	0.0204	0.0002	161	59	132	4	130	1
LMG-B5-15	76	637	854	0.75	0.0510	0.0012	0.1436	0.0036	0.0205	0.0001	239	56	136	3	131	1
LMG-B5-16	183	1381	965	1.43	0.0492	0.0008	0.1385	0.0026	0.0205	0.0003	167	39	132	2	131	2
LMG-B5-17	168	1298	1339	0.97	0.0497	0.0010	0.1397	0.0030	0.0205	0.0001	189	17	133	3	131	1
LMG-B5-18	42	332	530	0.63	0.0514	0.0008	0.1464	0.0027	0.0207	0.0001	261	32	139	2	132	1
LMG-B5-19	44	463	226	2.04	0.0528	0.0044	0.1475	0.0102	0.0205	0.0005	317	191	140	9	131	3
LMG-B5-20	163	861	1769	0.49	0.0513	0.0010	0.1468	0.0033	0.0208	0.0001	257	43	139	3	133	1
LMG-B5-21	258	1886	1054	1.79	0.0493	0.0009	0.1402	0.0029	0.0208	0.0001	167	47	133	3	133	1
LMG-B5-22	116	861	381	2.26	0.0514	0.0020	0.1437	0.0062	0.0204	0.0003	261	91	136	6	130	2
LMG-B5-23	210	1616	660	2.45	0.0487	0.0011	0.1363	0.0034	0.0204	0.0002	200	52	130	3	130	1

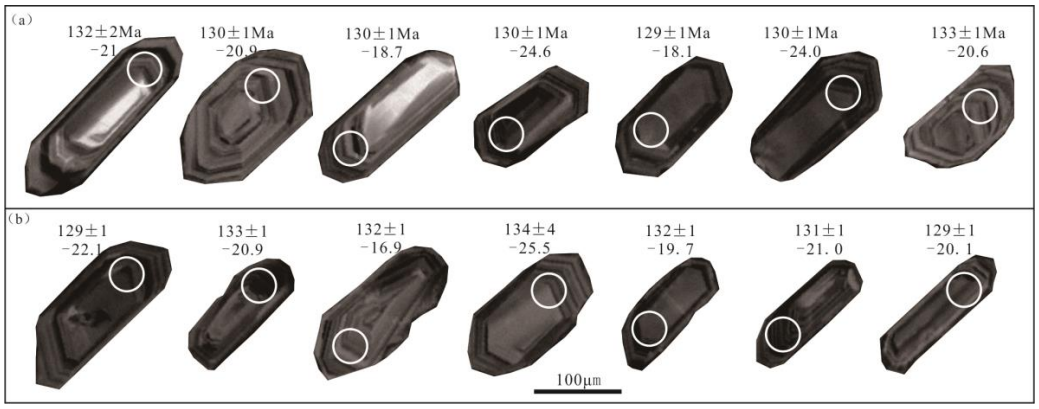

Figure 5. Zircon cathodoluminescence (CL) images of Leimengou granite porphyry (**a**) and monzonitic granite porphyry (**b**) with U–Pb ages and $\varepsilon_{Hf}(t)$.

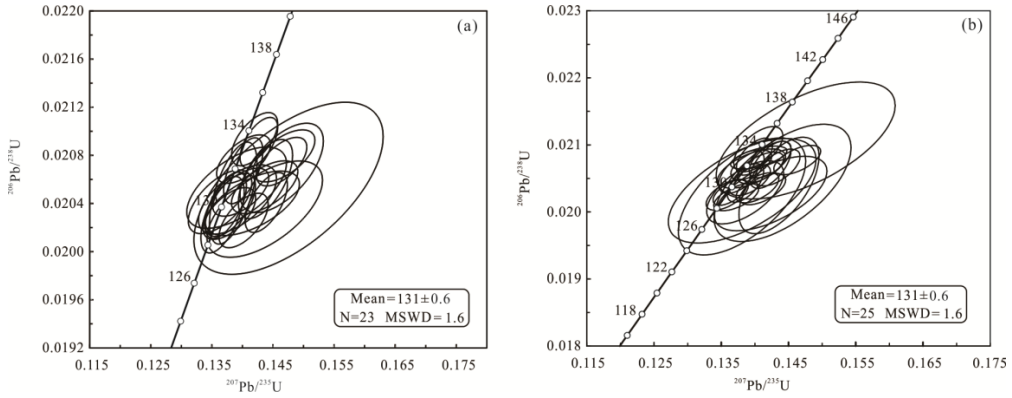

Figure 6. U–Pb Concordia diagram for the Leimengou granite porphyry zircons (**a**) and monzonitic granite porphyry zircons (**b**).

5.2. Whole Rock Major and Trace Elements Compositions

The analysis results for the major elements are shown in Table 2. It can be seen from the table that the Leimengou granite porphyry and monzonitic granite porphyry samples have similar and narrow major and trace elements compositions. Therefore, the non-separated description will be clear and perspicuous. The SiO_2 content of the samples is 68.55% to 70.36%. The content of Al_2O_3 is high, ranging from 14.08% to 15.32%. The contents of FeO^T, CaO and MgO are low, respectively 1.83% to 3.17%, 0.67% to 1.22%, and 0.27% to 0.32%. The content of K_2O is relatively high, ranging from 4.45% to 5.68%, the content of total alkali (K_2O + Na_2O) is between 7.84% and 9.07%, that of K_2O/Na_2O is 1.17–1.68. The Litman index δ value $[(K_2O + Na_2O)^2/(SiO_2 - 43)]$ is 2.3 to 3.13. The two rocks belong to the high-K calc-alkaline series according to the SiO_2–K_2O diagram (Figure 7a). The two rocks have the aluminum saturation index A/CNK of 1.06 to 1.28, so they belong to the peraluminous type (Figure 7b). The differentiation index (DI) of the rocks is from 87.8 to 92.0, indicating that the magma has a high degree of differentiation. Therefore, the Leimengou granite porphyry and monzonitic granite porphyry are characterized as high potassium, alkali-rich, low iron, poor in calcium and magnesium and supersaturated aluminum. The Late Mesozoic granite batholiths and most small porphyries on the southern margin of the North China Craton are quasi-aluminous, and a few small porphyries are peraluminous. In addition to the Leimengou granite porphyry, Jinduicheng and Balipu porphyries are included as well. These peraluminous porphyries are indistinguishable from quasi-aluminous granites in terms of genesis [12].

Table 2. Major elements (%) of the Leimengou granite porphyry and monzonitic granite porphyry.

Lithology	Granite Porphyry					Monzonitic Granite Porphyry					
Sample No.	**B16/LMG**	**B17/LMG**	**B18/LMG**	**B19/LMG**	**B20/LMG**	**B7/LMG**	**B8/LMG**	**B9/LMG**	**B10/LMG**	**B11/LMG**	**B12/LMG**
SiO_2	69.61	69.80	68.68	68.55	69.30	69.72	69.63	69.79	68.97	69.91	70.36
Al_2O_3	14.79	14.84	14.12	14.48	15.13	15.22	14.79	14.38	15.32	14.08	14.13
CaO	0.96	0.97	1.12	1.12	0.67	0.79	1.22	1.04	0.89	0.99	0.71
Fe_2O_3	1.81	1.86	2.90	2.86	0.86	2.03	2.32	1.74	1.55	0.96	2.43
FeO	0.31	0.31	0.56	0.18	1.06	0.23	0.14	0.46	0.49	1.02	0.22
K_2O	4.50	4.53	4.77	4.51	5.68	4.45	4.45	4.89	4.77	4.99	4.71
MgO	0.30	0.31	0.31	0.27	0.30	0.32	0.32	0.29	0.30	0.31	0.29
MnO	0.02	0.02	0.04	0.00	0.00	0.04	0.04	0.03	0.01	0.03	0.02
Na_2O	3.84	3.84	3.35	3.64	3.39	3.39	3.65	3.88	3.54	3.69	3.82
P_2O_5	0.09	0.10	0.09	0.09	0.09	0.11	0.09	0.09	0.11	0.10	0.10
TiO_2	0.26	0.25	0.25	0.27	0.26	0.24	0.26	0.26	0.25	0.25	0.26
LOI	1.73	1.72	2.46	2.46	1.99	2.09	2.01	1.82	1.84	1.77	2.04
Total	98.2	98.6	98.7	98.4	98.7	98.6	98.9	98.7	98.0	98.1	99.1
$K_2O + Na_2O$	8.34	8.37	8.12	8.15	9.07	7.84	8.10	8.77	8.31	8.68	8.53
K_2O/Na_2O	1.17	1.18	1.42	1.24	1.68	1.31	1.22	1.26	1.35	1.35	1.23
FeO^T	1.94	1.98	3.17	2.75	1.83	2.06	2.23	2.03	1.88	1.88	2.41
A/CNK	1.14	1.14	1.11	1.12	1.17	1.28	1.13	1.06	1.21	1.06	1.11
δ	2.6	2.6	2.6	2.6	3.1	2.3	2.5	2.9	2.7	2.8	2.7
DI	89.9	89.8	87.8	88.8	91.1	89.0	89.0	91.0	90.0	91.0	92.0
AR	3.3	3.3	3.3	3.2	3.7	2.5	2.7	3.0	2.6	2.9	3.1

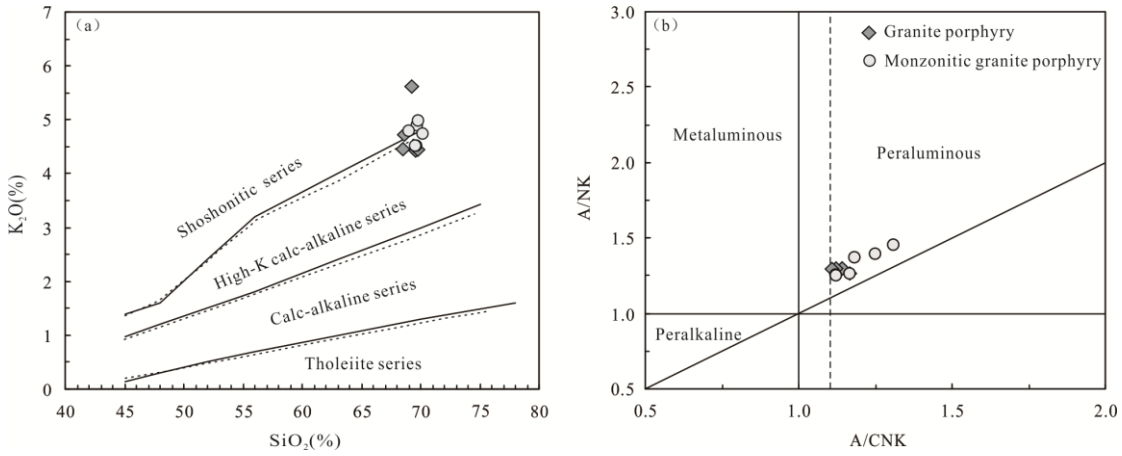

Figure 7. SiO_2 vs. K_2O (**a**) and A/CNK vs. A/NK (**b**) diagrams of the Leimengou granite porphyry and monzonitic granite porphyry (after Rickwood,1989 [22]; Peccerillo et al.,1976 [23]).

Table 3 lists the rare earth and trace element data for samples. The total rare earth content of the Leimengou monzonitic granite porphyry is 129 × 10^{-6} to 169 × 10^{-6}, which is lower than the average value of the upper crust (210.3 × 10^{-6}). The ratio of light to heavy rare earths, i.e., LREE/HREE, is 17.5 to 23.7, showing the characteristics of enrichment of LREEs and depletion of HREEs. The δ_{Eu} is 0.63 to 0.72, which is of moderate Eu depletion. There is no significant Ce abnormality and the δ_{Ce} is 0.92 to 1.05. The distribution pattern of REEs shows a right-leaning feature and a high degree of fractionation (Figure 8a). In terms of trace element content, large-ion lithophilic elements such as K, Rb, Ba, Sr, Th and U are enriched; high field strength elements such as Nb, Ti and P, and HREEs are significantly depleted (Figure 8b). The two rocks have almost the same distribution pattern of REEs and trace element standard changing curve (Figure 8).

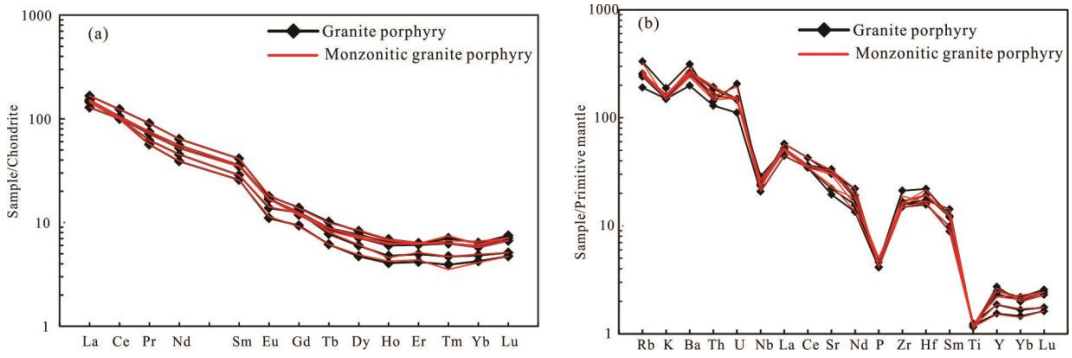

Figure 8. Chondrite-normalized REE patterns diagram (**a**) and primitive mantle normalized trace element spider diagram (**b**) for the Leimengou granite porphyry and monzonitic granite porphyry (normalization values after Sun et al., 1989 [24]).

5.3. Zircon Lu–Hf Isotopic Compositions

Lu–Hf isotopic analysis was performed on the zircons from the Leimengou granite porphyry and monzonitic granite porphyry samples. It was failed to get the isotopic composition of the measurement point No. 3 in granite porphyry sample. The results are shown in Table 4. Except for measurement points No. 6, 21, and 23 in the granite porphyry and measurement point No. 19 in the monzonitic granite porphyry, the zircons have a $^{176}Lu/^{177}Hf$ ratio of less than 0.002, suggesting that the zircon has very little radioactive Hf accumulation after formed, so the zircon $^{176}Hf/^{177}Hf$ ratio may be used to explore the Hf isotopic composition of the system in the process of rock formation [25–28].

Table 3. Trace elements(10^{-6})of the Leimengou granite porphyry and monzonitic granite porphyry.

Lithology	Granite Porphyry					Monzonitic Granite Porphyry					
Sample No.	**B16/LMG**	**B17/LMG**	**B18/LMG**	**B19/LMG**	**B20/LMG**	**B7/LMG**	**B8/LMG**	**B9/LMG**	**B10/LMG**	**B11/LMG**	**B12/LMG**
La	35.10	36.00	39.40	30.50	34.30	35.22	35.97	39.42	30.64	34.20	36.02
Ce	62.00	64.30	75.60	61.30	61.20	62.04	64.08	75.22	61.28	61.18	64.27
Pr	6.81	7.12	8.58	5.89	5.37	6.84	7.20	8.52	5.86	5.40	7.18
Nd	24.40	25.90	29.80	21.10	18.20	24.30	25.68	29.88	21.08	18.34	25.91
Sm	5.33	5.48	6.31	4.38	3.94	5.29	5.46	6.30	4.36	3.90	5.46
Eu	0.97	0.99	1.04	0.80	0.64	0.96	0.98	1.06	0.82	0.66	0.97
Gd	2.58	2.43	2.85	2.57	1.92	2.56	2.40	2.81	2.54	1.88	2.46
Tb	0.33	0.32	0.38	0.29	0.23	0.33	0.33	0.37	0.30	0.23	0.31
Dy	1.94	1.81	2.10	1.52	1.20	1.90	1.84	2.14	1.55	1.24	1.79
Ho	0.37	0.34	0.39	0.27	0.23	0.38	0.36	0.39	0.26	0.24	0.35
Er	1.02	1.01	1.05	0.82	0.69	1.04	1.02	1.06	0.85	0.72	1.03
Tm	0.18	0.16	0.16	0.12	0.10	0.19	0.17	0.16	0.12	0.09	0.16
Yb	1.08	1.01	0.98	0.82	0.72	1.06	1.12	0.98	0.84	0.70	1.02
Lu	0.19	0.18	0.17	0.13	0.12	0.18	0.18	0.17	0.13	0.12	0.18
Y	11.30	10.60	12.40	8.46	7.01	11.24	10.04	12.04	8.50	6.89	10.04
ΣREE	142	147	169	131	129	142	147	168	131	129	147
LREE/HREE	17.5	19.3	19.9	19.0	23.7	17.6	18.8	19.9	18.8	23.7	19.2
(La/Yb)N	23.3	25.6	28.8	26.7	34.2	23.8	23.0	28.9	26.2	35.0	25.3
δEu	0.71	0.72	0.65	0.67	0.63	0.70	0.71	0.67	0.69	0.66	0.70
δCe	0.92	0.93	0.96	1.05	0.99	0.92	0.92	0.96	1.05	0.99	0.92
Sc	2.12	2.37	2.09	1.31	1.74	1.73	1.86	0.97	1.40	2.09	1.91
V	14.10	14.40	13.40	12.20	23.20	15.64	14.58	16.27	13.46	22.82	13.44
Cr	7.61	10.10	6.92	4.48	1.59	6.89	4.56	8.42	5.75	7.16	2.09
Co	8.50	8.41	13.60	9.82	5.50	6.66	5.74	8.89	10.38	11.02	6.15
Ni	4.09	4.85	5.48	5.49	4.09	5.04	5.41	5.49	4.39	4.88	4.79
Cu	57.50	62.90	71.20	62.70	37.80	50.21	69.70	59.25	70.32	47.63	60.44
Zn	70.10	75.50	124.00	41.40	84.80	61.59	70.66	71.74	89.72	54.24	99.19
Ga	19.10	19.30	18.30	14.80	18.30	18.72	18.06	19.14	18.46	19.03	19.14
Rb	153	160	163	121	211	206	174	168	162	160	154
Sr	667	706	637	466	411	475	646	690	629	501	678
Zr	188	237	179	167	178	180	174	165	167	211	184
Nb	20.40	18.60	17.30	14.80	16.70	16.23	17.04	15.68	14.79	18.44	19.06
Mo	32.10	32.40	97.10	130.00	26.20	41.06	35.64	89.42	119.74	40.15	36.14
Cs	2.72	2.83	2.58	1.84	3.34	2.36	2.79	2.53	3.28	2.89	1.99
Ba	1857	1793	1766	1387	2191	1669	1740	1786	2009	1879	1824
Ta	0.94	0.94	0.81	0.73	0.84	0.81	0.74	0.95	0.84	0.78	0.76
Hf	5.91	6.78	5.35	4.86	5.03	6.68	5.94	5.24	4.96	5.11	6.04
Pb	49.60	59.40	89.40	27.00	50.00	51.08	79.84	56.46	34.05	50.14	61.19
Th	15.70	16.40	13.90	11.00	12.10	12.44	13.06	16.28	13.49	16.72	14.36
U	3.11	3.14	3.08	2.34	4.33	3.21	3.28	3.04	4.06	3.02	3.06

Table 4. Lu–Hf isotopic data of zircons from the Leimengou granite porphyry (LMG-B15) and monzonitic granite porphyry (LMG-B5).

Spot No.	Age (Ma)	$^{176}Yb/^{177}Hf$	$\pm 2\sigma$	$^{176}Lu/^{177}Hf$	$\pm 2\sigma$	$^{176}Hf/^{177}Hf$	$\pm 2\sigma$	$(^{176}Hf/^{177}Hf)_i$	$\varepsilon_{Hf}(t)$ *	t_{DM2}(Ma)	$f_{Lu/Hf}$
LMG-B15-1	129	0.048062	0.000584	0.001303	0.000014	0.282071	0.000016	0.282067	−22.1	2582	−0.96
LMG-B15-2	132	0.051009	0.000580	0.001551	0.000033	0.282213	0.000021	0.282209	−17.0	2266	−0.95
LMG-B15-4	132	0.038977	0.000659	0.000999	0.000017	0.282172	0.000017	0.282170	−18.4	2353	−0.97
LMG-B15-5	130	0.039045	0.000283	0.001196	0.000013	0.282068	0.000013	0.282065	−22.1	2586	−0.96
LMG-B15-6	133	0.098780	0.001511	0.002465	0.000038	0.282140	0.000021	0.282134	−19.7	2431	−0.93
LMG-B15-7	133	0.046918	0.000508	0.001406	0.000028	0.282120	0.000015	0.282116	−20.3	2472	−0.96
LMG-B15-8	131	0.040308	0.000289	0.001205	0.000012	0.282100	0.000013	0.282097	−21.0	2514	−0.96
LMG-B15-9	132	0.067944	0.001544	0.001831	0.000033	0.282094	0.000018	0.282089	−21.3	2531	−0.94
LMG-B15-10	133	0.040465	0.000533	0.001160	0.000011	0.282103	0.000015	0.282100	−20.9	2508	−0.97
LMG-B15-11	129	0.024340	0.001145	0.000729	0.000033	0.282125	0.000012	0.282123	−20.1	2459	−0.98
LMG-B15-12	129	0.048880	0.000934	0.001424	0.000016	0.282107	0.000014	0.282104	−20.8	2502	−0.96
LMG-B15-13	129	0.082936	0.001259	0.001962	0.000018	0.282106	0.000017	0.282101	−20.9	2506	−0.94
LMG-B15-14	130	0.039695	0.000831	0.001131	0.000021	0.282051	0.000014	0.282048	−22.8	2625	−0.97
LMG-B15-15	130	0.073319	0.000709	0.001848	0.000010	0.282058	0.000021	0.282053	−22.6	2612	−0.94
LMG-B15-16	133	0.051327	0.000675	0.001569	0.000046	0.282094	0.000017	0.282090	−21.2	2529	−0.95
LMG-B15-17	129	0.081835	0.001045	0.001944	0.000029	0.281907	0.000021	0.281903	−27.9	2946	-0.94
LMG-B15-18	130	0.051211	0.000478	0.001264	0.000019	0.282095	0.000017	0.282092	−21.2	2527	−0.96
LMG-B15-19	132	0.049832	0.001251	0.001216	0.000019	0.282215	0.000019	0.282212	−16.9	2259	−0.96
LMG-B15-20	134	0.056259	0.000781	0.001303	0.000016	0.282178	0.000020	0.282175	−18.2	2340	−0.96
LMG-B15-21	134	0.083829	0.000492	0.002012	0.000019	0.281972	0.000025	0.281967	−25.5	2800	−0.94
LMG-B15-22	130	0.075529	0.000173	0.001768	0.000017	0.281973	0.000023	0.281969	−25.6	2800	−0.95
LMG-B15-23	130	0.096849	0.002872	0.002130	0.000044	0.282116	0.000021	0.282111	−20.5	2484	−0.94
LMG-B15-24	130	0.042376	0.000848	0.001108	0.000017	0.282057	0.000015	0.282054	−22.5	2611	−0.97
LMG-B15-25	132	0.061336	0.000771	0.001599	0.000008	0.282137	0.000017	0.282133	−19.7	2434	−0.95
LMG-B5-1	132	0.058547	0.000203	0.001378	0.000003	0.282101	0.000015	0.282098	−21.0	2513	−0.96
LMG-B5-2	134	0.077725	0.000152	0.001750	0.000011	0.282089	0.000018	0.282085	−21.4	2541	−0.95
LMG-B5-3	133	0.038748	0.000689	0.000989	0.000009	0.282134	0.000013	0.282131	−19.7	2438	−0.97
LMG-B5-4	130	0.051489	0.000315	0.001363	0.000014	0.282103	0.000015	0.282099	−20.9	2510	−0.96
LMG-B5-5	130	0.051303	0.007587	0.001506	0.000156	0.282167	0.000024	0.282163	−18.7	2368	−0.95
LMG-B5-6	130	0.059494	0.000248	0.001558	0.000007	0.281977	0.000017	0.281956	−26.0	2827	−0.95
LMG-B5-7	130	0.071712	0.000357	0.001688	0.000023	0.282000	0.000016	0.281996	−24.6	2740	−0.95
LMG-B5-8	132	0.056462	0.002125	0.001445	0.000056	0.282131	0.000018	0.282127	−19.9	2447	−0.96
LMG-B5-9	130	0.061134	0.003106	0.001988	0.000061	0.282100	0.000020	0.282095	−21.1	2520	−0.94
LMG-B5-10	129	0.079758	0.000341	0.001554	0.000009	0.281068	0.000019	0.282179	−18.1	2333	−0.95
LMG-B5-11	130	0.082326	0.000535	0.001883	0.000007	0.281978	0.000020	0.282262	−15.2	2149	−0.94
LMG-B5-12	131	0.093100	0.001976	0.001879	0.000029	0.282081	0.000023	0.282077	−21.7	2560	−0.94
LMG-B5-13	131	0.078480	0.003446	0.001539	0.000072	0.282075	0.000024	0.282071	−21.9	2572	−0.95
LMG-B5-14	130	0.048948	0.000592	0.001096	0.000014	0.282015	0.000018	0.282013	−24.0	2703	−0.97
LMG-B5-15	131	0.040535	0.002433	0.001140	0.000019	0.282145	0.000023	0.282197	−17.5	2293	−0.97
LMG-B5-16	131	0.080707	0.000905	0.001915	0.000051	0.282107	0.000027	0.282102	−20.8	2504	−0.94

Table 4. *Cont.*

Spot No.	Age (Ma)	$^{176}Yb/^{177}Hf$	±2σ	$^{176}Lu/^{177}Hf$	±2σ	$^{176}Hf/^{177}Hf$	±2σ	$(^{176}Hf/^{177}Hf)_i$	$\varepsilon_{Hf}(t)$ *	t_{DM2}(Ma)	$f_{Lu/Hf}$
LMG-B5-17	131	0.037668	0.000609	0.001026	0.000017	0.282043	0.000014	0.282040	−23.0	2642	−0.97
LMG-B5-18	132	0.055958	0.000781	0.001368	0.000016	0.282100	0.000015	0.282096	−21.0	2516	−0.96
LMG-B5-19	131	0.079309	0.000492	0.002033	0.000019	0.282089	0.000018	0.282084	−21.5	2544	−0.94
LMG-B5-20	133	0.039725	0.000831	0.001145	0.000021	0.282109	0.000017	0.282106	−20.6	2494	−0.97
LMG-B5-21	133	0.072211	0.000709	0.001769	0.000010	0.282088	0.000017	0.282084	−21.4	2543	−0.95
LMG-B5-22	130	0.044137	0.000289	0.001247	0.000012	0.282099	0.000020	0.282096	−21.0	2517	−0.96
LMG-B5-23	130	0.067784	0.001544	0.001842	0.000033	0.282093	0.000021	0.282088	−21.3	2535	−0.94

* $\varepsilon_{Hf}(t) = \{[(^{176}Hf/^{177}Hf)_s - (^{176}Lu/^{177}Hf)_s \times (e^{\lambda t} - 1)]/[(^{176}Hf/^{177}Hf)_{CHUR,0} - (^{176}Lu/^{177}Hf)_{CHUR} \times (e^{\lambda t} - 1)] - 1\} \times 10{,}000$; $t_{DM2} = 1/\lambda \times \ln\{1 + [(^{176}Hf/^{177}Hf)_{s,t} - (^{176}Hf/^{177}Hf)_{DM,t}]/[(^{176}Lu/^{177}Hf)_C - (^{176}Lu/^{177}Hf)_{DM}]\} + t$; $f_{Lu/Hf} = [(^{176}Lu/^{177}Hf)_s/(^{176}Lu/^{177}Hf)_{CHUR}] - 1$; $(^{176}Lu/^{177}Hf)_s$ and $(^{176}Hf/^{177}Hf)_s$ are measured values; $(^{176}Hf/^{177}Hf)_{CHUR,0} = 0.282793$, $(^{176}Lu/^{177}Hf)_{CHUR} = 0.0338$, $(^{176}Hf/^{177}Hf)_{DM} = 0.28325$, $(^{176}Lu/^{177}Hf)_{DM} = 0.0384$; $\lambda = 1.867 \times 10^{-11}a^{-11}$, $(^{176}Lu/^{177}Hf)_C = 0.015$, t = Zircon U–Pb age.

The granite porphyry and monzonitic granite porphyry have similar Lu–Hf isotopic compositios. For the granite porphyry, the $^{176}Hf/^{177}Hf$ ratios of 24 measurement points vary from 0.281907 to 0.282215. The Hf isotope initial ratio $(^{176}Hf/^{177}Hf)_i$ calculated from the corresponding zircon U–Pb age is from 0.281903 to 0.282212. The Hf isotopic compositions vary widely, with the $\varepsilon_{Hf}(t)$ values changing from −27.9 to −16.9, mainly from −23 to −20. The two-stage model age is t_{DM2} = 2259 to 2946 Ma, mainly within the range of 2400 to 2700 Ma.

For the monzonitic granite porphyry, the $^{176}Hf/^{177}Hf$ ratios of 23 measurement points vary from 0.281068 to 0.282163. The Hf isotope initial ratio $(^{176}Hf/^{177}Hf)_i$ is from 0.281956 to 0.282262. The $\varepsilon_{Hf}(t)$ values also vary widely, changing from −26.0 to −15.2, mainly from −22 to −20. The two-stage model age is t_{DM2} = 2149 to 2827 Ma, mainly within the range of 2500 to 2600 Ma.

6. Discussion

6.1. Timing of Magmatism

According to the previous research results, the age of the Leimengou granite porphyry is 136.2 ± 1.5 Ma, which is obviously earlier than that of the Leimengou Mo deposit (131.6 ± 2.0–133.1 ± 1.9 Ma) [9]. It is considered that the time scale of the granite magmatism from partial melting to invasion and the final consolidation cooling is less than 0.1 Ma [29,30], and the petrogenesis and mineralization should be simultaneous on the geological time scale. In this study, the LA-(MC)-ICP-MS zircon U–Pb ages for the Leimengou granite porphyry and monzonitic granite porphyry are 131 ± 0.6 Ma, completely consistent with the mineralization age, which proves the simultaneity of the diagenesis and mineralization.

About six km northwest of Leimengou intrusion, the Huashan granite batholith is exposed. Surrounding it, there are a series of granite intrusions (including the Leimengou intrusion), dykes, and cryptoexplosive breccias, which were once considered as the products of the differentiation of the Huashan batholith [31]. Then, for the age of the Leimengou granite porphyry (136.2 ± 1.5 Ma [9]) is significantly earlier than that of the Huashan granite batholith (131 ± 1–132 ± 2 Ma [7]), the Leimengou Mo-bearing porphyry is considered not to be related to the Huashan batholith [10]. In this study, the age of the Leimengou porphyry is coeval with that of the Huashan granite batholith. Therefore, the rock-forming time cannot be used to negate the genetic relationship between the two. On the contrary, the results of this study confirm the spatial and temporal consistency between the two. In the eastern Qinling molybdenum ore belt, there is a close spatial-temporal correlation between the ore-bearing porphyries and the adjacent batholiths. The spatial-temporal consistency between the Leimengou ore-bearing porphyry and the Huashan batholith is consistent with this general phenomenon.

6.2. Petrogenesis and Magma Sources

Wang et al. (2011) [12] classified the late Mesozoic granites from the Qinling into the Late Jurassic-Early Cretaceous (160–130 Ma) and the mid-late Cretaceous (120–100 Ma) stages. The Leimengou intrusion yield zircon U–Pb age of 131 ± 0.6 Ma, indicating that the rocks should be the first-stage product. At the southern margin of the North China Block, the first stage of the Late Jurassic-Early Cretaceous (160–130 Ma) was dominated by I-type granites with minor I-A transitional type, and the majority of the rocks had A/CNK = 0.9–1.0. It belongs to quasi-aluminous type, and most of the rocks are peraluminous [12].

The aluminum saturation index A/CNK of Leimengou intrusion is 1.06 to 1.28, belonging to the peraluminous type, which is different from most of the granites in the southern margin of the North China Block during the same period. If A/CNK = 1.1 is the boundary between type I and type S, then the Leimengou intrusion belongs to S type granite. However, in mineralogy, the dark-colored mineral in the rocks is mainly biotite and does not contain aluminiferous minerals such as muscovite and garnet, and the characteristic minerals of A-type granites, i.e., alkaline dark-colored minerals. Considering that the rock has a high differentiation index (DI = 89–92), the identification of the rock

type, i.e., I, S, or A type of the Leimengou intrusion will be difficult [28], therefore, the classification of granites by Barbarin (1990, 1996, 1999) [32–34] is referenced.

Barbarin (1990; 1996; 1999) [32–34] classified granites into seven rock types based on their rock properties, mineral compositions, geochemistry, and isotope characteristics. They were respectively muscovite peraluminous granites (MPG), bluestone and rich biotite peraluminous granites (CPG), potassium-rich and potassium-feldspar porphyritic calc-alkaline granites (KCG), amphibole calc-alkaline granitoids (ACG), and island arc-porphyry basaltic granites (ATG), thoracic granites (RTG) and overbased and alkaline granites (PAG). Leimengou intrusion is located in the Taihua Group. There are no mafic microgranular enclave in the outcrop, and there is no obvious deformation; biotite is rich and no muscovite is found; in terms of rock type, they belong to granite porphyry and monzonitic granite porphyry. The rock is peraluminous with A/CNK of 1.06 to 1.28, and has a high differentiation index (DI). These characteristics indicate that the Leimengou intrusion belongs to the CPG type according to the Barbarin (1990,1996,1999) classification [32–34]. The CPG is a deep-melt effect of the "dry" rock through hot mantle magma under-plating or penetrating, that is, the heat of partial melting is mainly provided by the under-plating or mantle-derived magma injected into the crust [35]. It is now widely believed that the Late Mesozoic granite porphyry and related Mo deposits on the southern margin of the North China Block were formed by under-plating of basic magmatism under intra-plate geodynamic conditions [1,35]. Obviously, this undermining provided enough heat to partially melt the source rock and form magma. However, it needs further confirmation whether mantle-derived substances added into the the magma in the partial melting process.

The Leimengou intrusion belongs to peraluminous high-K calc-alkaline series. In the chondrite-normalized REE patterns diagrams, the rock has the right-leaning feature with light rare earth enrichment and obvious differentiation between LREEs and HREEs. The rock shows the moderate Eu negative anomaly (δ_{Eu} = 0.63–0.72), is enriched with large ionic lithophilic elements such as K, Rb, Ba, Sr, Th and U, and depleted with high field strength elements such as Nb, Ti and P. These characteristics indicate that the Leimengou intrusion has a clear "crust" imprint, and its material source should be mainly crust-derived. The Zr/Hf ratio is 26.9 to 41.3, which is between the crust average and the mantle average. The value reflects the contribution of mantle source materials, suggesting that some mantle materials may participate in the formation of the Leimengou intrusion.

The granite porphyry and monzonitic granite porphyry of the Leimengou intrusion have similar Lu–Hf isotopic compositions, with $\varepsilon_{Hf}(t)$ values varying from −27.9 to−16.9 and −26.0 to −15.2, respectively, and both concentrating on the range of −23 to −20. In the Hf isotopic evolution diagram (Figure 9), all the sample points of the two rocks are between 1.8 Ga crust and 3.6 Ga crust evolution line far away from the chondrite evolution line, which also indicates that the source material of the Leimengou intrusion is mainly the ancient crust-derived material. The granite porphyry and monzonitic granite porphyry have the two-stage model age (t_{DM2}) of 2259 to 2946 Ma and 2149 to 2827 Ma, and are mainly concentrated within the range of 2400 to 2700 Ma and 2500–2600 Ma, respectively, indicating that the source material is mainly the Neoarchean crust component. In the southern margin of North China Block, the mid-late Cretaceous (120–100 Ma) granites also have large variations in zircon $\varepsilon_{Hf}(t)$ values (ranging from −26.3 to −13.5) and two-stage model age(ranging from 2040 to 2860 Ma) [12], which is consistent with the Leimengou granitic rocks. Previous studies on the zircon U–Pb and Ar–Ar geochronology of the crystalline basement Taihua Group on the southern margin of the North China Block indicate that the formation time of the Taihua Group was about 2700 Ma, and the metamorphism occurred within the range of 2200 to 2300 Ma [36,37].It can be concluded that the Taihua Group is probably the main source region of the Leimengou intrusion. However, the Leimengou granitic rocks show large variations in zircon $\varepsilon_{Hf}(t)$ values (11 ε units), suggesting more than one sources. According to the Lu–Hf isotopic composites of tonalite- trondhjemite-granodiorite gneisses of the Taihua Group ($^{176}Hf/^{177}Hf$ = 0.281195 to 0.281497, $^{176}Lu/^{177}Hf$ = 0.000861 to 0.001688, $^{176}Yb/^{177}Hf$ = 0.041713 to 0.084714 [38], the calculated $\varepsilon_{Hf}(t)$ values using the age of 131 Ma (age of the Leimengou intrusion) is from −51.3 to −42.4, which are

far less than those of the Leimengou intrusion. Therefore, some juvenile components may participate in the magmatic process.

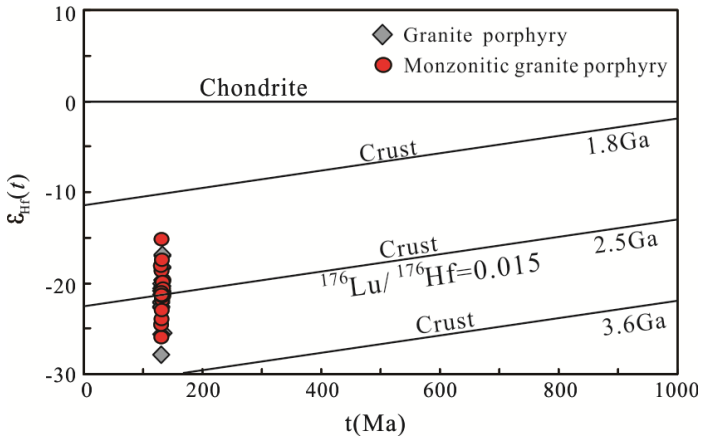

Figure 9. Diagram of $\varepsilon_{Hf}(t)$-t(Ma) for the Leimengou granite porphyry and monzonitic granite porphyry.

The source of the ore-forming material and fluids of the prphyry deposits is largely similar to the source of magma. Although the above-mentioned geochemical and isotope results of the Leimengou intrusion have given the information of crust source being the main source, previous studies on the ore-forming materials and fluids of the Leimengou Mo deposit revealed the addition of mantle-derived components. According to the Re content of molybdenite in the Leimengou Mo deposit (11.5×10^{-6} to 16.2×10^{-6}), Li et al. (2006) [9] believed that the ore-forming materials in the deposit mainly derived from the lower crust, mixed with a small amount of mantle components. The C and O isotopes indicate that deep-source components have been added to the ore-forming fluids of the Leimengou deposit, and the Pb isotope characteristics of the altered potassium feldspar further indicate that mantle components have been added to the ore-forming fluids [39]. Both the ore-forming materials and fluids in the Leimengou deposit have the addition of mantle-derived components, possibly suggesting that the source region of the Leimengou intrusion is mixed with mantle-derived components. This is consistent with the material source of Late Mesozoic granite intrusions on the southern margin of the North China Block, which was summarized by Wang et al. (2011) [12]. They believed that the source materials of these granites were likely to be the Taihua Group, but were generally added the mantle-derived components, and the mantle-derived materials were probably from the under plating of the Yanshanian basal magmatism in Eastern China.

In summary, the Leimengou intrusion was derived mainly from the partial melting of ancient crustal material (most likely the Taihua Group) and has been mixed with a small amount of mantle-derived components.

7. Conclusions

(1) Both the granite porphyry and the monzonitic granite porphyry, related to the Leimengou Mo mineralization, yield the LA-(MC)-ICP-MS zircon U–Pb ages of 131 ± 0.6 Ma (MSWD = 1.6), which is consistent with the molybdenite Re–Os age of the Leimengou deposit. The age is also consistent with the petrogenesis age of the Huashan granite batholith.

(2) The whole rock geochemistry and zircon Lu–Hf isotopic indicate that the source material of the Leimengou intrusion is mainly from the ancient continental crust, likely the Archean Taihua Group, with a small amount of mantle-derived components.

Author Contributions: J.C., H.Y., X.C., W.H. and P.W. made field investigation. J.C. performed the zircon U–Pb dating and Lu–Hf isotope analysis, interpreted all the data and finished the original draft of the paper.

H.Y. reviewed the original draft of paper and acted as the project administration. X.C. collected and provide the geological maps and W.H. performed the whole-rock geochemical analysis. P.W. drew the diagrams and corrected the language.

Funding: This study was financially supported by the Central Public-interest Scientific institution Basal Research Fund (No. YYWT-201713) and received no external funding.

Acknowledgments: We gratefully thank Hou Kejun, Guo Chunli et al. from the Institute of Mineral Resources, Chinese Academy of Geological Sciences for their important guidance and assistance in zircon age testing, Hf isotope testing, and data analysis.

Conflicts of Interest: The authors declare no conflict of interest.

References

1. Lu, X.X.; Yu, Z.P.; Feng, Y.L.; Wang, Y.T.; Ma, W.F.; Gui, H.F. Mineralization and tectonic setting of the deep-hypabyssal granites in East Qinling Mountain. *Miner. Depos.* **2002**, *21*, 168–178, (In Chinese with English abstract).
2. Ye, H.S.; Mao, J.W.; Li, Y.F.; Guo, B.J.; Zhang, C.Q.; Liu, W.J.; Yan, Q.R.; Liu, G.Y. SHRIMP zircon U–Pb and molybdenite Re-Os dating for the super large Donggou porphyry Mo deposit in East Qinling, China and its geological implication. *Acta Geol. Sin.* **2006**, *80*, 1078–1088, (In Chinese with English abstract).
3. Dai, B.Z.; Jiang, S.Y.; Wang, X.L. Petrogenesis of the granitic poyphyry related to the giant molybdenum deposit in Dong gou, Henan Province, China: Constraints from petrogeochemistry, zircon U–Pb chronology and Sr–Nd–Hf isotopes. *Acta Geol. Sin.* **2009**, *25*, 2889–2901, (In Chinese with English abstract).
4. Huang, F.; Luo, Z.H.; Lu, X.X.; Gao, F.; Chen, B.H.; Yang, Z.F.; Pan, Y.; Li, D.D. Was Donggou porphyry Mo deposit derived from Taishanmiao batholith? *Miner. Depos.* **2009**, *28*, 569–584, (In Chinese with English abstract).
5. Zhao, H.J.; Mao, J.W.; Ye, H.S.; Hou, K.J.; Liang, H.S. Chronology and petrogenesis of Shijiawan granite porphyry in Shannxi Province: Constrains from zircon U–Pb geochronology and Hf isotopic compositions. *Miner. Depos.* **2010**, *29*, 143–157, (In Chinese with English).
6. Feng, Y.Q.; Qian, Z.Z.; Zhang, J.J.; Cui, Z.H.; Jiang, C.; Meng, D.M. Metallogenic regularity of Yanshanian intermediate-acid small intrusions in East Qinling. *J. Earth Sci. Environ.* **2014**, *36*, 128–140, (In Chinese with English abstract).
7. Mao, J.W.; Xie, G.Q.; Pirajno, F.; Ye, H.S.; Wang, Y.B.; Li, Y.F.; Xiang, J.F.; Zhao, H.J. Late Jurassic-Early Cretaceous granitoid magmatism in Eastern Qinling, central-eastern China: SHRIMP zircon U–Pb ages and tectonic implications. *Aust. J. Earth Sci.* **2010**, *57*, 51–78. [CrossRef]
8. Chen, X.D.; Ye, H.S.; Mao, J.W.; Wang, H.; Chu, S.T.; Cheng, G.X; Liu, Y.W. Characteristics of ore-forming fluids of the Leimengou porphyry Mo depoit, western Henan Province, and its geological significance. *Acta Geol. Sin.* **2011**, *85*, 1629–1642, (In Chinese with English abstract).
9. Li, Y.F.; Mao, J.W.; Liu, D.Y.; Wang, Y.B.; Wang, Z.L.; Wang, Y.T.; Li, X.F.; Zhang, Z.H.; Guo, B.J. SHRIMP zircon U–Pb and molybdenite Re-Os datings for the Leimengou porphyry molybdenum deposit, western Henan and its geological implication. *Geol. Rev.* **2006**, *52*, 122–131, (In Chinese with English abstract).
10. Su, J.; Zhang, B.L.; Sun, D.H.; Cui, M.L.; Qu, W.J.; Du, A.D. Geological features and Re-Os isotopic dating of newly discovered Shapoling veinlet-disseminated Mo deposit in the Eastern Section of East Qinling mountains and its geological significance. *Acta Geol. Sin.* **2009**, *83*, 1490–1496, (In Chinese with English abstract).
11. Zhang, G.W.; Zhang, B.R.; Yuan, X.C.; Xiao, Q.H. *Qinling Belt and Continental Dynamics*; Science Press: Beijing, China, 2001; pp. 1–729. (In Chinese)
12. Wang, X.X.; Wang, T.; Qi, Q.J.; Li, S. Temporal-spatial variations, origin and their tectonic significance of the Late Mesozoic granites in the Qinling, Central China. *Acta Petrol. Sin.* **2011**, *27*, 1573–1593, (In Chinese with English abstract).
13. Fan, H.R.; Xie, Y.H.; Wang, Y.L. Petrological and geochemical characteristics and genesis of the Huashan granitic batholith, Western Henan. *Acta Petrol. Mineral.* **1994**, *13*, 19–32, (In Chinese with English abstract).
14. Xiao, E.; Hu, J.; Zhang, Z.Z.; Dai, B.Z.; Wang, Y.F.; Li, H.Y. Petrogeochemistry, zircon U–Pb dating and Lu–Hf isotopic compositions of the Haoping and Jinshanmiao granites from the Huashan complex batholith in eastern Qinling Orogen. *Acta Petrol. Sin.* **2012**, *28*, 4031–4046, (In Chinese with English abstract).
15. Zhang, Y.H. Alteration and the Forming Dynamic Process of the Qiyugou Breccia Gold Deposit. Ph.D. Thesis, China University of Geosciences in Beijing, Beijing, China, 2006.

16. Liu, Y.S.; Hu, Z.C.; Zong, K.Q.; Gao, C.G.; Gao, S.; Xu, G.J.; Chen, H.H. Reappraisement and refinement of zircon U–Pb isotope and trace element analyse by LA-ICP-MS. *Chin. Sci. Bull.* **2010**, *55*, 1535–1546. [CrossRef]
17. Sláma, J.; Košler, J.; Condon, D.J.; Crowley, J.L.; Gerdes, A.; Hanchar, J.M.; Horstwood, M.S.A.; Morris, G.A.; Nasdala, L.; Norberg, N.; et al. Plešovice zircon—A new natural reference material for U–Pb and Hf isotopic microanalysis. *Chem. Geol.* **2008**, *249*, 1–35. [CrossRef]
18. Nasdala, L.; Hofmeister, R.W.; Norberg, N.; Martinson, J.M.; Corfu, F.; Dörr, W.; Kamo, S.L.; Kennedy, A.K.; Kronz, A.; Reiners, P.W.; et al. Zircon M257-a homogeneous natural reference material for the ion microprobe U–Pb analysis of zircon. *Geostand. Geoanal. Res.* **2008**, *32*, 247–265. [CrossRef]
19. Hou, K.J.; Li, Y.H.; Tian, Y.R. In situ U–Pb zircon dating using laser ablation-multi ion counting-ICP-MS. *Miner. Depos.* **2009**, *28*, 481–492, (In Chinese with English abstract).
20. Hou, K.J.; Li, Y.H.; Zou, T.R.; Qu, X.M.; Shi, Y.R.; Xie, G.Q. Laser ablation-MC-ICP-MS technique for Hf isotope microanalysis of zircon and its geological applications. *Acta Petrol. Sin.* **2007**, *23*, 2595–2604, (In Chinese with English abstract).
21. Elhlou, S.; Belousova, E.; Griffin, W.L.; Pearson, N.J.; O'reilly, S.Y. Trace element and isotopic composition of GJ-red zircon standard by laser ablation. *Geochim. Cosmochim. Acta* **2006**, *70*, A158. [CrossRef]
22. Rickwood, P.C. Boundary lines within petrologic diagrams which use oxides of major and minor elements. *Lithos* **1989**, *22*, 247–263. [CrossRef]
23. Peccerillo, A.; Taylor, S.R. Geochemistry of Eocene calc-alkaline volcanic rocks from the Kastamonu area, Northern Turkey. *Contrib. Mineral. Petrol.* **1976**, *58*, 63–81. [CrossRef]
24. Sun, S.S.; McDonough, W.F. Chemical and isotope systematics of oceanic basalts: Implications for mantle composition and processes. Saunders A D. Magmatism in Ocean Basins. *Geol. Soc. Publ.* **1989**, *42*, 313–345. [CrossRef]
25. Patchett, P.J.; Kouvo, O.; Hedge, C.E.; Tatsumoto, M. Evolution of continental crust and mantle heterogeneity: Evidence from Hf isotope. *Contrib. Mineral. Petrol.* **1981**, *78*, 279–297. [CrossRef]
26. Knudsen, T.L.; Griffin, W.L.; Hartz, E.H.; Andresen, A.; Jackson, S. In-situ hafnium and lead isotope analyses of detrital zircons from the Devonian sedimentary basin of NE Greenland: A record of repeated crustal reworking. *Contrib. Mineral. Petrol.* **2001**, *141*, 83–94. [CrossRef]
27. Kinny, P.D.; Maas, R. Lu–Hf and Sm-Nd isotope systems in zircon. *Rev. Mineral. Geochem.* **2003**, *53*, 327–341. [CrossRef]
28. Wu, F.Y.; Li, X.H.; Yang, J.H.; Gao, S.; Zheng, Y.F. Discussions on the petrogenesis of granites. *Acta Petrol. Sin.* **2007**, *23*, 1217–1238, (In Chinese with English abstract).
29. Petford, N.; Cruden, A.R.; McCaffrey, K.J.W. Vigneresse, J.L. Granite magma formation, transport and emplacement in the Earth's crust. *Nature* **2000**, *408*, 669–673. [CrossRef] [PubMed]
30. Turner, S.; Costa, F. Measuring timescales of magmatic evolution. *Elements* **2007**, *3*, 267–272. [CrossRef]
31. Shao, K.Z.; Wang, B.D. Au mineralization and metallogenic regularity in northwestern Songxian County, Henan Province. *Henan Geol.* **1992**, *10*, 161–167. (In Chinese)
32. Barbarian, B. Granitoids: Main petrogenetic classification in relation to origin and tectonic setting. *Geol. J.* **1990**, *25*, 227–238. [CrossRef]
33. Barbarian, B. Genesis of the two main types of peraluminous granitoids. *Geology* **1996**, *24*, 295–298. [CrossRef]
34. Barbarian, B. A review of the relationships between granitoid types, their origins and their geodynamic environments. *Lithos* **1999**, *46*, 605–626. [CrossRef]
35. Xiao, Q.H.; Deng, J.F.; Ma, D.S. *The Methods of Investigation on Granitoids*; Geological Publishing House: Beijing, China, 2002; pp. 1–293. (In Chinese)
36. Ni, Z.Y.; Wang, R.M.; Tong, Y.; Yang, C.; Dai, C.M. $^{207}Pb/^{206}Pb$ age of zircon and $^{40}Ar/^{39}Ar$ of amphibole from plagioclase amphibolite in the Taihua Group, Luoning, Henan, China. *Geol. Rev.* **2003**, *19*, 361–366, (In Chinese with English Abstract).
37. Diwu, C.R.; Sun, Y.; Lin, C.L.; Wang, H.L. LA-(MC)-ICP-MS U–Pb zircon geochronology and Lu–Hf isotope compositions of the Taihua complex on the southern margin of the North China Craton. *Chin. Sci. Bull.* **2010**, *55*, 2557–2571. [CrossRef]

38. Diwu, C.R.; Sun, Y.; Lin, C.L.; Liu, X.M.; Wang, H.L. Zircon U–Pb ages and Hf isotopes and their geological significance of Yiyang TTG gneisses from Henan Province, China. *Acta Petrol. Sin.* **2007**, *23*, 253–262, (In Chinese with English Abstract).
39. Chen, X.D. Characteristics of Ore-Forming Fluids and Metallogenesis in the Leimengou Porphyry Molybdenum Deposit, Western Henan Province. Master's Thesis, China University of Geosciences in Beijing, Beijing, China, 2012.